

# First High-Angular Resolution $L'$ Images of the $\beta$ Pictoris Debris Disc with the VLT / NaCo

Julien Milli<sup>1,2</sup>, Dimitri Mawet<sup>1</sup>, Olivier Absil<sup>3</sup>, Anne-Marie  
Lagrange<sup>2</sup>, David Mouillet<sup>2</sup>, Julien H. Girard<sup>1</sup>  
and Jean-Charles Augereau<sup>2</sup>

<sup>1</sup>ESO, Alonso de Cordova 3107, Casilla 19001, Santiago 19, Chile, email: [jmilli@eso.org](mailto:jmilli@eso.org)

<sup>2</sup>IPAG, University Joseph Fourier, CNRS, BP 53, 38041, Grenoble, France

<sup>3</sup>AGO, Université de Liège, 17 Allée du Six Août, B-4000 Liège, Belgium

**Abstract.** Imaging debris discs in the  $L'$ -band ( $3.8 \mu\text{m}$ ) is a difficult task. Quasi-static speckles from imperfect optics prevail below  $1''$  whereas background emission is the dominant noise source beyond that separation and is much larger than at shorter wavelengths. We demonstrate here the potential of the newly commissioned AGPM coronagraph on VLT/NaCo combined with advanced star and sky subtraction technique based on Principal Component Analysis, and we analyze the morphology of the  $\beta$  Pictoris disc.

**Keywords.** stars: individual ( $\beta$  Pictoris), techniques: high angular resolution, techniques: image processing

## 1. Introduction

Circumstellar discs are the birthplace of planets, especially the inner regions within a few tens of astronomical units. Imaging discs at that scale requires high-contrast and high-angular resolution techniques, as well as specific data reduction tools. Innovative methods such as Angular Differential Imaging, ADI (Marois *et al.* 2006) or Principal Components Analysis, PCA, (Soummer *et al.* 2012) were developed to detect and characterize faint companions. For discs, they are also used to reveal high spatial frequency features, e.g. Lagrange *et al.* (2012), but any extended structure is strongly biased (Milli *et al.* 2012). On the specific example of the  $\beta$  Pictoris system imaged with the VLT/NaCo, we present here a way to correct the biases induced by ADI and analyze the morphology of the disc in the  $L'$ -band.

## 2. Observations and data reduction specific to the disc geometry

The star  $\beta$  Pictoris was observed on January, 31 2013 with the AGPM coronagraph that operates in the  $L'$ -band at  $3.8 \mu\text{m}$  (see D. Mawet *et al.*, these proceedings). The star and background subtraction algorithm consisted in a PCA performed in four concentric annuli, retaining 5 components out of 90. The disc is detected from  $0.5''$  to  $4.5''$  at a mean  $3\sigma$  level (Fig. 1). A low-frequency noise due to the strong and variable background emission prevents the detection beyond  $4.5''$ . The warp seen at smaller wavelengths between 3 and  $5''$  (Lagrange *et al.* 2012) is marginally detected on the South-West (SW) side at  $3''$ .

## 3. Morphological analysis and discussion

We estimated the position angle (PA) of each side of the disc by derotating the image to align each side horizontally so that the disc spine centers are zero on average between  $1''$  and  $3''$  (Lagrange *et al.* 2012). The measured PA is  $28.3^\circ \pm 2^\circ$  and  $212.3^\circ \pm 2^\circ$  for the NE and SW sides respectively. This is the first time the PA is measured in such a close separation range, the NE value is compatible with measurements at shorter wavelengths

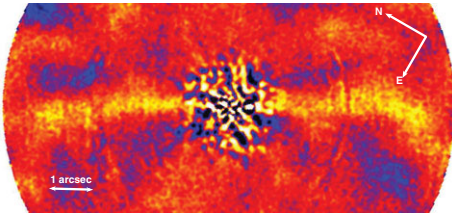


**Figure 1.** AGPM coronagraphic image. The colour scale is linear.

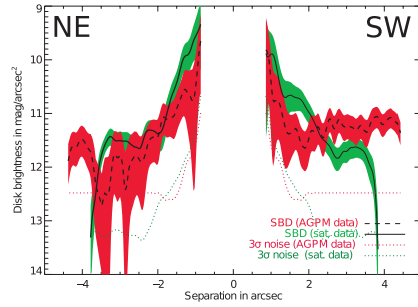


**Figure 2.** Disc SBD with error bars in colours.

and larger separations whereas the SW side is only marginally compatible. We interpret this as the superimposition of the warp component and preferential forward scattering on the SW side above the midplane. The surface brightness distribution (SBD) corrected from the flux losses related to ADI (see section 4) is shown in Fig. 2. We overplotted the same analysis performed on non-coronagraphic, saturated, NaCo archival data taken in the same band on September, 28 2010. Although the low-frequency background noise is lower, the observing strategy implied telescope offsets that limit the field of view to  $3.5''$  in radius and bright speckles and diffraction residuals from the telescope spiders prevent clear conclusions below  $1''$ . Both images agree on a smooth SBD between  $1''$  and  $3''$  on the NE side, with a power-law index of  $-1.0$ . Golimowski *et al.* (2006) measured indices of  $-1.45$ ,  $-1.43$  and  $-1.38$  for observations at 435 nm, 606 nm, and 814 nm respectively. Therefore these observations confirm that the SBD gets flatter at larger wavelengths. The brightness asymmetry detected in the coronagraphic image between  $3''$  and  $4''$  and seen in mid-infrared at  $8.7 \mu\text{m}$  by Telesco *et al.* (2005) is not confirmed on the non-coronagraphic image.

#### 4. Modelisation of the disc and correction of the ADI biases

A careful calibration of flux losses was performed using disc models generated with the GRaTeR code (Augereau *et al.* 1999). We assumed a radially symmetric distribution of optically thin dust with constant scattering cross-section. The radial distribution is described by two power-laws of exponent  $\alpha_{in} = 2$  and  $\alpha_{out} \leq 0$  with a peak density at the radius  $r_0$ . The disc model is subtracted from the initial data cube which is then re-reduced using PCA. We repeated this step iteratively by varying the free parameters of the disc model until the residuals are minimized. We performed this minimization for three discrete disc inclinations  $i$  ( $91^\circ$ ,  $95^\circ$ , and  $100^\circ$ ) and both isotropic and anisotropic scattering. The best reduced  $\chi^2$  is obtained with an isotropic model of a disc having  $i = 95^\circ$ ,  $PA = 30.3^\circ \pm 0.8^\circ$ ,  $r_0 = 35.6^{+20}_{-5} \text{ AU}$  and  $\alpha_{out} = -0.7 \pm 0.2$ . The peak density radius  $r_0$  is poorly constrained. The best disc model was then used to calibrate the flux losses resulting from the PCA reduction ( $0.9 \text{ mag/arcsec}^2$  at  $2''$ ) and to correct the SBD in Fig. 2.

#### References

- Augereau, J. C., Lagrange, A. M., Mouillet, D., Papaloizou, J. C. B., & Grorod, P. A. 1999, *A&A*, 348, 557
- Golimowski, D. A., Ardila, D. R., Krist, J. E., *et al.* 2006, *AJ*, 131, 3109
- Lagrange, A.-M., Boccaletti, A., Milli, J., *et al.* 2012, *A&A*, 542, A40
- Marois, C., Lafrenière, D., Doyon, R., Macintosh, B., & Nadeau, D. 2006, *ApJ*, 641, 556
- Milli, J., Mouillet, D., Lagrange, A.-M., *et al.* 2012, *A&A*, 545, A111
- Soummer, R., Pueyo, L., & Larkin, J. 2012, *ApJ*, 755, L28
- Telesco, C. M., Fisher, R. S., Wyatt, M. C., *et al.* 2005, *Nature*, 433, 133